

Central Lancashire Online Knowledge (CLOK)

Title	Spectrochemical analyses of growth phase-related bacterial responses to low (environmentally-relevant) concentrations of tetracycline and nanoparticulate silver
Type	Article
URL	https://clock.uclan.ac.uk/21321/
DOI	https://doi.org/10.1039/C7AN01800B
Date	2018
Citation	Jin, Naifu, Semple, Kirk T., Jiang, Longfei, Luo, Chunling, Zhang, Dayi and Martin, Francis L (2018) Spectrochemical analyses of growth phase-related bacterial responses to low (environmentally-relevant) concentrations of tetracycline and nanoparticulate silver. The Analyst. ISSN 0003-2654
Creators	Jin, Naifu, Semple, Kirk T., Jiang, Longfei, Luo, Chunling, Zhang, Dayi and Martin, Francis L

It is advisable to refer to the publisher's version if you intend to cite from the work.
<https://doi.org/10.1039/C7AN01800B>

For information about Research at UCLan please go to <http://www.uclan.ac.uk/research/>

All outputs in CLOK are protected by Intellectual Property Rights law, including Copyright law. Copyright, IPR and Moral Rights for the works on this site are retained by the individual authors and/or other copyright owners. Terms and conditions for use of this material are defined in the <http://clock.uclan.ac.uk/policies/>

**Spectrochemical analyses of growth phase-related bacterial responses
to low (environmentally-relevant) concentrations of tetracycline and
nanoparticulate silver**

Naifu Jin¹, Kirk T. Semple¹, Longfei Jiang², Chunling Luo², Dayi Zhang^{1,3,*}, Francis
L. Martin^{4,*}

¹*Lancaster Environment Centre, Lancaster University, Lancaster LA1 4YQ, UK;*

²*Guangzhou Institute of Geochemistry, Chinese Academy of Sciences, Guangzhou
510640, China;*

³*School of Environment, Tsinghua University, Beijing 100084, China;*

⁴*School of Pharmacy and Biomedical Sciences, University of Central
Lancashire, Preston PR1 2HE, UK;*

***Corresponding authors:**

Francis L Martin, School of Pharmacy and Biomedical Sciences, University of
Central Lancashire, Preston PR1 2HE, UK; Email: flmartin@uclan.ac.uk

Dayi Zhang, School of Environment, Tsinghua University, Beijing 100084, China;
Email: d.zhang@lancaster.ac.uk

22 **Abstract**

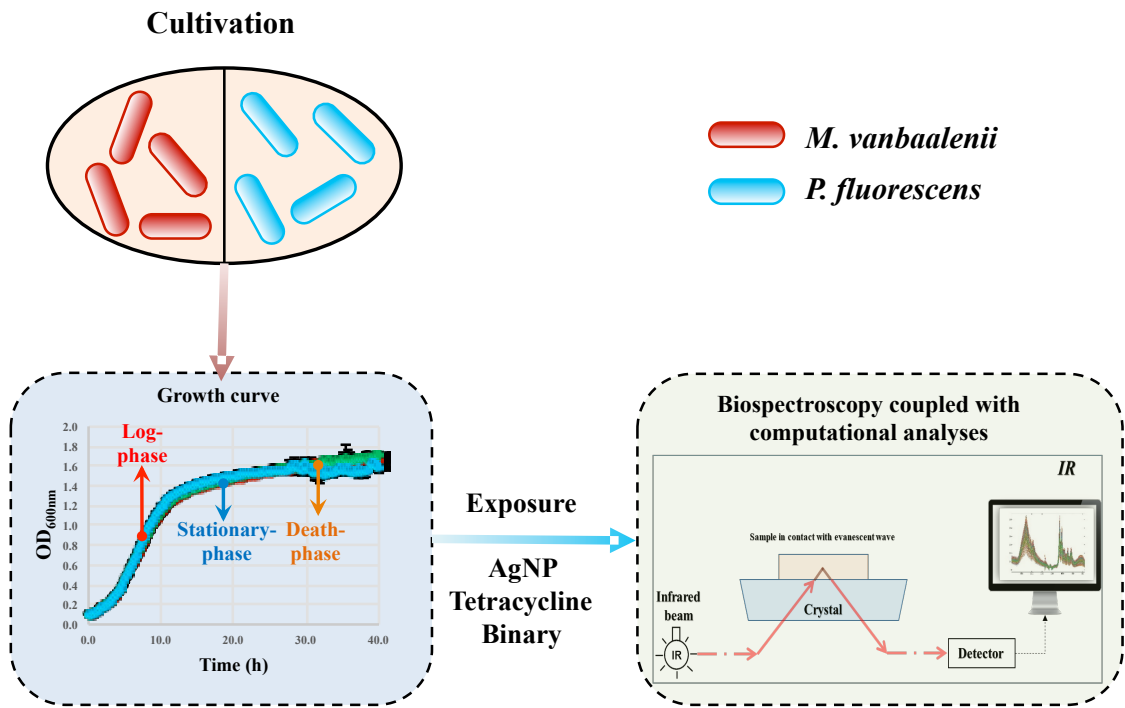
23 Exposure to environmental insults generally occurs at low levels, making it
24 challenging to measure bacterial responses to such interactions. Additionally,
25 microbial behaviour and phenotype varies in differing bacterial types or growth
26 phases, likely giving rise to growth- or species-specific responses to environmental
27 stimuli. The present study applied a spectrochemical tool, infrared (IR) spectral
28 interrogation coupled with multivariate analysis, to investigate the growth- and
29 species-specific responses of two bacterial strains, Gram-negative *Pseudomonas*
30 *fluorescens* and Gram-positive *Mycobacterium vanbaalenii*, to low concentrations of
31 tetracycline, nanoparticulate silver (AgNP) or mixtures thereof. Results indicate the
32 tendency for tetracycline-induced biospectral alterations to occur in outer-cellular
33 components, *e.g.*, phospholipids or proteins, while AgNPs-induced changes are
34 mainly associated with proteins ($\sim 964\text{ cm}^{-1}$, $\sim 1485\text{ cm}^{-1}$, $\sim 1550\text{ cm}^{-1}$, ~ 1650
35 cm^{-1}). The primary altered targets are correlated with bacterial membranes or
36 outer-cellular components. Furthermore, significant lipid changes at $1705\text{-}1750\text{ cm}^{-1}$
37 were only present in *P. fluorescens* cells compared to *M. vanbaalenii*, owing to
38 differences in cell wall structure between Gram-positive and -negative bacteria. This
39 study also found distinct biospectral alterations in non-log phase compared to log
40 phase, confirming bacterial growth-dependent responses to environmental exposures.
41 It implies that previous studies on log phase only may underestimate the impacts from
42 exposures of interest *in situ*, where bacteria stay in different growth stages. Our work
43 proves the feasibility of biospectroscopy in determining bacterial responses to
44 low-level environmental exposures in a fast and efficient manner, revealing sufficient
45 biochemical information continuously through growth phases. As a nondestructive
46 approach, biospectroscopy may provide deeper insights into the actual and *in situ*
47 interactions between microbes and environmental stimuli, regardless of the exposure
48 level, growth phase, or bacterial types.

49

50 **ToC graphic**

51

52



53

54

55 **Introduction**

56 The impacts of environmental insults on microorganisms have been widely studied.
57 Antibiotics are a group of antimicrobial agents capable of causing environmental
58 insults of major concern from both a scientific and public perspective. A significant
59 number and quantity of antibiotics have been extensively applied in human and
60 veterinary medicine¹. Various means by which these drugs and their metabolites enter
61 the environment post-excretion have been examined. The most common way by
62 which antibiotics are discharged is *via* sewage treatment plants with ultimate release
63 into surface or groundwater. Previous studies point to >40 different categories of
64 antibiotics found in groundwater and even drinking water, ranging from nanogram per
65 liter to microgram per liter¹⁻⁴. Strikingly, residues of veterinary antibiotics enter the
66 environment in a much more direct way through application of liquid manure as
67 fertilizer^{5, 6}.

68 Additionally, nanoparticles (NPs) may also pose high risks to our living
69 environment. Nanoparticulate silver (AgNP) is one of the most widely-used NPs,
70 occurring in analytical pathogen-detecting devices, as antibacterial additives in
71 commercial products (clothing, food containers, wound dressings, implant coatings,
72 and refrigerators), and in ultrafiltration membranes for water purification⁷⁻⁹. The
73 abuse and widespread usage of antibiotics and AgNPs may exacerbate risks of
74 antimicrobial resistance¹⁰. Although many studies have addressed such consequences
75 in living microorganisms, they usually employ very high-level exposures of
76 antibiotics and AgNPs in the laboratory, generally 100- or even 1000-fold greater than
77 exposures in real-world scenarios. Thus, the *in-vitro* outcome of high-level exposure
78 in reflecting real-world impacts is always questioned^{11, 12}.

79 Bacteria play a critical role in geochemical processes and are ubiquitously present
80 in the environment as a unique group of microorganisms. They can be used
81 advantageously to study the impacts of environmental exposures, but their
82 communities are incredibly complicated with regards to composition, functions and
83 dynamics¹³⁻¹⁶. Gram staining depending on cell membrane structure, for instance, is
84 the general classification method for categorizing bacteria into Gram-positive or
85 -negative groupings. The fundamental difference between these two categories is
86 membrane structure, *i.e.*, there is only a thin peptidoglycan layer (~2-3 nm) between
87 the cytoplasmic membrane and the outer membrane of Gram-negative bacteria while

Gram-positive bacteria exhibit a thick peptidoglycan layer of 30 nm but lack an outer membrane¹⁷. Differing attributes of membrane structure may result in distinct responsive behaviors towards environmental exposures, for instance towards toxicity and anti-biocide actions¹⁸. Additionally, growth phase is another major concern in studying bacterial communities. Bacterial growth is typically divided *via* growth rate, *i.e.*, lag phase, acceleration phase, exponential phase (log-phase), retardation phase, stationary phase, and phase of decline. In previous studies, log-phase has been the most investigated, but this condition is seldom found in the natural environment due to rarity of optimal growth conditions¹⁹. Instead, stationary- to death-phase representing nutrient depletion circumstances may be more representative²⁰.

To date, a wide range of techniques have been used to assess bacterial responses to environmental exposures, such as Christensen test-tube method (CTT)^{21, 22}, Congo red agar method (CRA)²³, IcaADB gene detection using polymerase chain reaction (PCR)^{24, 25}, and pulsed-field gel electrophoresis (PFGE)^{26, 27}. However, these approaches target specific endpoints and are not feasible for diagnosing bacterial responses to environmental exposures. CTT and CRA primarily require access to pure cultures. The others are molecular-based, defining the genotype of a whole community rather than the individual phenotype or behavior. For instance, distinguishing the functions or behaviours of individual bacterial cells within a bacterial biofilm is almost impossible *via* molecular-based methods, owing to the enormous diversity of bacterial strains and complexity in community structure. Additionally, these approaches have to be performed under restrictive laboratory conditions²⁸⁻³⁰, making it unachievable to discriminate bacterial phenotypes within complex bacterial communities in real environmental samples. Therefore, an increasing need for novel high-throughput approaches is raised, allowing one to analyze the real environmental microbiota *in situ* *via* a non-destructive means.

Biospectroscopy has a long history of application in microbiology since the 1960s^{31, 32}. Attributes of biospectroscopy include non-destructive, non-invasive, high-throughput and label-free, which provide many advantages for the investigation of environmental and biochemical dynamic changes in low-level exposure circumstances. In recent studies, biospectroscopy has proved sensitive to physiological and morphological alterations resulted from low-level environmental exposures³³⁻³⁵. Specifically, infrared (IR) spectroscopy exploits the principle that

biochemical bonds perform some degree of vibrations induced by stretching, bending, scissoring or twisting after energy absorption at particular wavelengths. The “biochemical-cell fingerprint” region is located within the mid-IR region, which is the most information-rich about biochemical structures³⁶. Through assessing derived spectral peaks or alterations, *i.e.*, bio-fingerprints, the biochemical structure of interrogated targets can be revealed³⁷⁻³⁹. Additionally, Raman spectroscopy, as a complementary method to IR, can provide information on chemical bonds and composition even under a hydrated environment^{40, 41}. Furthermore, another merit of biospectroscopy over other techniques is that it allows investigations to be undertaken *in situ* in real-time, which can generate continuous biochemical information through the entire biological processes rather than only obtaining static results from specific time points.

As a broad-spectrum of antibiotic, tetracycline is effective against both Gram-positive and -negative bacteria with only a few exceptions⁴², having a history of several decades usage in animal feeds and consequently probably more ubiquitous in the natural environment than other in-house antibiotics (*e.g.*, kanamycin)⁴³. The present study therefore chose tetracycline as the studied antibiotic, discriminating and assessing bacterial responses to tetracycline and AgNPs *via* biospectroscopy coupled with multivariate analysis. Additionally, recent studies have reported the synergistic antibacterial effects of antibiotics and metals or NPs⁴⁴, *e.g.*, amoxicillin and AgNPs⁴⁵, but its effects on bacterial physiology remains unclear. Our work also considered and interrogated microbial responses to the binary-exposure of tetracycline and AgNPs *via* IR spectroscopy. Regarding the real-world scenario, our results distinguished the distinct biospectral alterations in different bacterial types and growth phases, helping one to understand the bacterial behaviour post-exposure to low-level antimicrobials. We aim to demonstrate that biospectroscopy approaches can characterise physiological features of bacteria and lend profound insights into the relationship between these and bacterial responses to environmental insults.

Materials and methods

Sample preparation

Unless stated otherwise, all the chemicals used in this study were purchased from Sigma-Aldrich (UK). The AgNPs (catalogue no. 730785, Sigma-Aldrich, UK) have a 10-nm particle size at a stock concentration of 0.02 mg/mL, dissolved in aqueous buffer with sodium citrate as stabilizer. Two classic soil bacterial strains, *Mycobacterium vanbaalenii* PYR-1 (Gram-positive) and *Pseudomonas fluorescens* (Gram-negative), were selected owing to their ubiquity and wide distribution in the soil environment and their well-known physiological behaviour^{36, 46-48}. These two strains were cultured in Luria-Bertani (LB) broth at 30±2°C with 150 rpm shaking for 24 h. Bacterial growth was measured every 10 min by optical density at 600 nm (OD₆₀₀) with a microplate reader (FLUOstar Omega, BMG Labtech, UK). AgNPs, tetracycline or AgNPs-tetracycline mixture was added into cell suspensions in early log-phase (OD₆₀₀=0.6), respectively. To mimic the low-level exposure in natural environment⁴⁹⁻⁵², the exposure concentration was set as 4 µg/L for AgNPs and 1 µg/L for tetracycline. One millilitre of bacterial suspension was taken 2, 8 and 24 h post-exposure, representing log-phase, stationary-phase and death-phase, respectively. For each sample, bacterial cells were harvested by centrifugation at 4000 relative centrifugal force (rcf) for 5 min, and the cell pellets were subsequently washed three times with sterile deionized water and 70% ethanol to fix bacteria and remove residues of growth media. The fixed samples were then applied onto Low-E slides for subsequent spectrochemical analysis.

Spectrochemical analysis

IR spectra were acquired *via* a Bruker TENSOR 27 FTIR spectrometer (Bruker Optics Ltd., UK) equipped with a Helios ATR attachment containing a diamond internal reflection element (IRE). Instrument parameters were set at 32 scans and 16 cm⁻¹ resolution. A total number of 30 spectra were acquired per sample through the ATR magnification-limited viewfinder camera. Before measuring each new specimen, the crystal was cleaned with deionized water, and background readings were retaken.

Raman spectra were acquired *via* an InVia Renishaw Raman spectrometer (Renishaw Inc. Gloucester, Gloucestershire, UK). After calibration, sample slides were placed on an operating stage (a Renishaw automated 100 nm encoded XYZ

stage), and a 50× objective (numeral aperture 0.75) was applied to focus on the cell pellet. The parameters of measurement included: grating scan type (extended); spectrum range (400 to 1800 cm^{-1}); configuration (Laser, 785 nm edge); grating (1200 l/mm 633/790); exposure time (30 s); accumulations (1); and, laser power (100%). When all the parameters were set up, a map measurement was used for analyzing each colony. The spectrometer's entrance slit of 50 μm combined with a 1200 lines/mm ($\sim 1.0 \text{ cm}^{-1}$ spectral resolution) diffraction grating dispersing Raman signals onto a master Renishaw Pelletier cooled charge coupled detector (CCD). A white light camera mounted on the microscope was used to obtain the darkfield images and visualize locations for spectral acquisition. For each captured picture of a cell pellet, 25 spectra were randomly obtained.

Spectrochemical data processing

All the initial data generated from ATR-FTIR spectroscopy were analyzed using MATLAB R2011a (TheMathsWorks, Natick, MA, USA) coupled with the IRootLab toolbox (<http://irootlab.googlecode.com>)⁵³. The acquired IR spectra were cut to the biochemical-cell fingerprint region (1800 - 900 cm^{-1}), undertaken rubberband baseline correction and normalized to Amide I (1650 cm^{-1}). Multivariate analysis of principal component analysis-linear discriminant analysis (PCA-LDA) was applied to the pre-processed data to derive ten uncorrelated principal components (PCs) from acquired spectra, which account for >99% of the total variance and also maximize inter-class variance whilst minimizing intra-class variance⁵⁴⁻⁵⁶. Cross-calculation was subsequently performed to mitigate risk resulting from LDA overfitting⁵⁷. The PCA-LDA loadings using (n-1) samples (n = number of samples in dataset) was trained *via* leave-one-out cross-validation and then calculated the scores of the rest sample. This process was performed for all scores within the test. To investigate roles of reactive oxygen species (ROS) in antibiotic action and resistance, the CySS-to-protein ratio was calculated from derived Raman spectra by dividing the intensity of cysteine band (CySS, 668 cm^{-1}) by that of protein band (1447 cm^{-1})³⁴.

Statistical analysis

Statistical significance of differences and variance analysis (*P*-value <0.05) of biospectral alterations among different treatments of bacterial types and growth phases was performed using one-way analysis of variance (ANOVA) with Tukey's

post-hoc test. All statistical analyses were carried out in GraphPad Prism 6. Multivariate regression trees (MRT) were used to analyze the influence of bacterial type, growth phase and exposure on biospectral alterations using the R package “mvpart”. Herein, Gram-positive (*M. vanbaalenii*) and Gram-negative (*P. fluorescens*) strains were assigned as 1 and 0. For growth phase, the log-phase, stationary-phase, and death-phase were assigned as 1, 2 and 3, respectively. The exposure of AgNPs, tetracycline and their mixtures were assigned as 1, 2 and 3, respectively.

Results and discussion

Growth curves post-exposure to AgNPs and tetracycline

Growth curves (Figure 1) for *M. vanbaalenii* (Figure 1A) and *P. fluorescens* (Figure 1B) show that both strains exhibit approximately a 3 h lag-phase and the log-phase starts some 3.5 h after initial culture. Both enter the stationary-phase at approximately 11 h ($OD_{600}=1.2$). After about 30 h culture, significant fluctuations indicate the death phase stage for both strains. There was no significant difference regarding the growth between control (non-exposure) and exposure groups ($P > 0.05$). Although previous work reports a remarkable inhibition of bacterial growth post-exposure to AgNPs⁵⁸, the exposure levels herein (4 ng/mL) are much lower than the previous study (10-100 $\mu\text{g/mL}$) and it therefore appeared not to significantly impact either bacterial strain. Similarly, low concentrations of tetracycline did not induce any apparent changes on the respective growth curves either. A previous study reports that *Synechocystis* sp. exposure to 1 $\mu\text{g/L}$ of tetracycline for five days exhibited no apparent effect, possibly because of natural variability in tetracycline resistance⁵⁹. Additionally, *M. vanbaalenii* and *P. fluorescens* are both environmental bacteria widespread in natural habitats (water and soil), and they are reported to tolerate insults from low-level exposures of antimicrobials³⁶. Thus, their growth curves are hardly affected by low-level exposures to AgNPs or tetracycline.

Growth-dependent spectrochemical alterations derived from IR spectra

Raw spectra reveal very limited information because low-level exposures may only induce miniscule alterations (Figure 1C and 1D). Multivariate analysis assists in highlighting the spectral changes and key distinguishing biomarkers representing

spectral differences. Previous studies indicate that most features align along linear discriminant one (LD1), which includes most of the spectral information (Figure 2)^{34, 36}. The observed segregation in PCA-LDA scores plots (Figure 2A and 2E) is significant ($P < 0.05$), indicating distinct biospectral alterations between the growth phases. The results of one-way ANOVA [see Electronic Supporting Information (ESI) Table S1 and S2] also demonstrate the statistically significant means of all segregation categories in each growth phase ($P < 0.05$).

Biospectral discriminant peaks and their tentative assignments illustrate the interactions between cellular components in different growth stages (Figure 3). The spectra of *M. vanbaalenii* show a broad range of variations in stationary-phase compared to log-phase (Figure 3A), including glycogen ($\sim 1018 \text{ cm}^{-1}$), carbohydrate ($\sim 1165 \text{ cm}^{-1}$), symmetric phosphate stretching vibrations ($\nu_s \text{PO}_2^-$; $\sim 1088 \text{ cm}^{-1}$), COO-symmetric stretching vibrations of fatty acids and amino acid ($\sim 1377 \text{ cm}^{-1}$), lipid ($\sim 1701 \text{ cm}^{-1}$), and proteins ($\sim 1474 \text{ cm}^{-1}$)⁶⁰. The main discriminant peaks in death-phase include Amide I ($\sim 1650 \text{ cm}^{-1}$), Amide II ($\sim 1550 \text{ cm}^{-1}$), glycogen ($\sim 1018 \text{ cm}^{-1}$), and proteins ($\sim 1481 \text{ cm}^{-1}$)^{36, 60}. In contrast, the major spectral features of *P. fluorescens* are identical in stationary-phase and death-phase (Figure 3E), mainly comprising proteins and lipids, *i.e.*, Amide I ($\sim 1650 \text{ cm}^{-1}$), Amide II ($\sim 1550 \text{ cm}^{-1}$), and lipids ($1705\text{-}1750 \text{ cm}^{-1}$)^{34, 35}. For both strains, the degrees of all the growth-related alterations illustrate an increasing tendency from stationary-phase to death-phase, possibly attributed to cellular differentiation under nutrient depleted conditions in stationary-phase and death-phase, which cause the changing cell wall structure to adapt to growth circumstances^{20, 61, 62}. The spectral differences between the two strains is principally contributed by cell membrane structure in that Gram-negative bacteria contain two lipid-associated bilayers compared to Gram-positive cells¹⁷. The extra membrane in Gram-negative strains (*P. fluorescens*) might increase more detectable alterations related to proteins and lipids across growth phases.

Spectrochemical alterations with AgNPs/tetracycline exposure

Although the exposures herein are low-level, characterizable effects can be identified post-exposure to AgNPs, tetracycline or their mixtures *via* biospectroscopy coupled with multivariate analysis. The key alterations in *M. vanbaalenii* post-exposure to AgNPs include glycogen ($\sim 1022 \text{ cm}^{-1}$), proteins ($\sim 1485 \text{ cm}^{-1}$), $\nu_s \text{PO}_2^-$ ($\sim 1088 \text{ cm}^{-1}$,

1092 cm^{-1}), carbohydrate ($\sim 1165 \text{ cm}^{-1}$), lipids ($\sim 1705 \text{ cm}^{-1}$, 1709 cm^{-1}), Amide I ($\sim 1670 \text{ cm}^{-1}$), and protein phosphorylation ($\sim 964 \text{ cm}^{-1}$) (Figure 3B)^{33, 36}. Tetracycline exposure led to discriminating alterations in *M. vanbaalenii* in Amide III ($\sim 1269 \text{ cm}^{-1}$), protein phosphorylation ($\sim 964 \text{ cm}^{-1}$), glycogen ($\sim 1022 \text{ cm}^{-1}$), Amide I ($\sim 1609 \text{ cm}^{-1}$, 1612 cm^{-1} , 1659 cm^{-1}), COO- symmetric stretching vibrations of fatty acids and amino acid ($\sim 1408 \text{ cm}^{-1}$), and lipids ($\sim 1701 \text{ cm}^{-1}$, 1713 cm^{-1})⁶⁰ (Figure 3C). However, for *P. fluorescens*, the biomarkers in both individual treatments are further concentrated on proteins ($\sim 1650 \text{ cm}^{-1}$, $\sim 1550 \text{ cm}^{-1}$) and lipids ($1705\text{-}1750 \text{ cm}^{-1}$)^{34, 36} (Figure 3F and 3G).

In binary exposure treatments, more complex profile differences in spectral alterations in ATR-FTIR spectra are observed. The primary changes in *M. vanbaalenii* are consistent with proteins ($\sim 1650 \text{ cm}^{-1}$) and lipids ($1705\text{-}1750 \text{ cm}^{-1}$) in all growth phases (Figure 3D)^{34, 36}. In contrast, the exposure-associated spectral alterations in *P. fluorescens* vary significantly with growth phase (Figure 3H), *e.g.*, the biomarkers in stationary-phase with binary effects include glycogen ($\sim 1053 \text{ cm}^{-1}$), Amide I ($\sim 1609 \text{ cm}^{-1}$), COO- symmetric stretching vibrations of fatty acids and amino acid ($\sim 1389 \text{ cm}^{-1}$), asymmetric phosphate stretching vibrations ($\nu_{\text{as}}\text{PO}_2^-$; $\sim 1196 \text{ cm}^{-1}$), lipid ($\sim 1732 \text{ cm}^{-1}$), and Amide II ($\sim 1508 \text{ cm}^{-1}$)^{35, 60}. They change to lipid ($\sim 1709 \text{ cm}^{-1}$ and 1751 cm^{-1}), Amide I ($\sim 1609 \text{ cm}^{-1}$), Amide II ($\sim 1543 \text{ cm}^{-1}$), $\nu_{\text{as}}\text{PO}_2^-$ ($\sim 1211 \text{ cm}^{-1}$) and glycogen ($\sim 1053 \text{ cm}^{-1}$)^{36, 60} in death-phase.

In general, most spectral alterations post-exposure are associated with lipids and proteins indicating bacterial cell membranes are primary targets, probably because tetracycline or AgNPs penetrate bacterial cells *via* passive diffusion and inhibits bacterial growth by disturbing protein synthesis or altering membrane structure⁶³. Through growth phases, Gram-negative bacteria inhibit a broad range of alterations associated with lipids, *e.g.*, ($1705 - 1750 \text{ cm}^{-1}$), which is absent in Gram-positive bacteria, mainly attributed to their different cell wall composition. The rigidity and extended cross-linking may reduce target sites on cell wall for environmental exposure and increase difficulties in antimicrobial penetration⁴⁴.

Factors influencing spectrochemical alteration

From conducted spectral analysis, factors inducing IR spectral alterations can be classified as intrinsic and external categories. The inherent one includes bacterial type

(Gram-positive or Gram-negative) and growth phase, and the external category refers to the types of exposure. These factors function and interact simultaneously, with distinct impacts on microbial responses to environmental exposures. To quantify the importance of each factor, multivariate regression tree (MRT) analysis was conducted through the isolated discriminating biomarkers (characteristic peaks). The MRT graph illustrates the relationship of spectral variations and impact factors with four splits according to bacterial types, growth phase and exposure groups, explaining 90.8% of spectral variance (Figure 5).

Spectral variation is first split by bacterial type which accounts for 65.6% of the total variation, owing to more changes associated with membrane components observed in *P. fluorescens* (Gram-negative) than *M. vanbaalenii* (Gram-positive), e.g., proteins and phospholipid-derived fatty acids. Multivariate analysis also illustrates various spectrochemical alterations between *P. fluorescens* and *M. vanbaalenii*. For example, significant lipid changes ($1705\text{-}1750\text{ cm}^{-1}$) present in *P. fluorescens* treatments are absent in *M. vanbaalenii* treatments. The cell membrane of Gram-negative bacteria contains two lipid associated bilayers, which is likely to increase the influence of applied exposure on the cell wall structure, while there is only one lipid bilayer in the membrane and a thick ring of peptidoglycan and teichoic acid of Gram-positive bacteria¹⁷. This difference may influence the structural integrity and eventually the microbial response to external stimuli. Furthermore, both Gram-positive and -negative bacteria from stationary phase show a comprehensive range of alterations in cellular components (i.e., Amide I, II, III, $\nu_{\text{as}}\text{PO}_2^-/\nu_{\text{s}}\text{PO}_2^-$, glycogen, carbohydrates, lipids, etc.; Figure 6), indicating many underlying biological activities. This can be primarily attributed to a growing cell wall from log to stationary phase, which increases the amounts of membrane components⁶⁴ and induces changes on the surface of the bacterial envelope and protein synthesis²⁰. Such changes may have considerable influence on the rigidity of the cells, resistance to environmental changes, as well as immunochemical properties. Results of both MRT and multivariate analyses therefore suggest bacterial type as the primary intrinsic factor determining IR alterations post-exposure to AgNP or tetracycline.

Growth phase also shows significant impacts on bacterial spectra after environmental exposure. The Gram-negative group is further split in the MRT graph by growth phase (i.e., log-phase vs. stationary-phase and death-phase), owing to

increasing alterations of membrane components along with the growth stage, which explains 13.2% of total variation (Figure 5). Similarly, multivariate analysis demonstrates the same growth-dependent results. Post-exposure to AgNP for instance, the spectra of both strains in log-phase are clearly separated from those in stationary-phase or death-phase (Figure 2B-D). The induced alterations from growth phases are associated with various cellular components. Specifically in log-phase, IR spectral biomarkers reflecting the major alterations of *M. vanbaalenii* post-exposure to AgNP are Amide I ($\sim 1612\text{ cm}^{-1}$), COO⁻ symmetric stretching vibrations of fatty acids and amino acids ($\sim 1381\text{ cm}^{-1}$), lipid ($\sim 1717\text{ cm}^{-1}$), glycogen ($\sim 1011\text{ cm}^{-1}$), $\nu_{\text{as}}\text{PO}_2^-$ ($\sim 1215\text{ cm}^{-1}$), and carbohydrate ($\sim 1165\text{ cm}^{-1}$) (Figure 6A)^{36, 60}. However, samples from stationary-phase exhibit a contrasting profile consisting only of alterations of proteins ($\sim 1377\text{ cm}^{-1}$) and Amide I, II, III ($\sim 1609\text{ cm}^{-1}$, 1566 cm^{-1} , 1254 cm^{-1}) (Figure 6B)³³. In tetracycline or tetracycline-AgNP mixture treatments, the most-induced biomarkers in log-phase shift to proteins, *i.e.*, Amide I ($\sim 1163\text{ cm}^{-1}$, 1616 cm^{-1}), Amide II ($\sim 1520\text{ cm}^{-1}$, 1558 cm^{-1}) and Amide III ($\sim 1327\text{ cm}^{-1}$) (Figure 6A)³³, but they are associated more with cellular components in stationary-phase, including Amide I ($\sim 1589\text{ cm}^{-1}$), Amide II ($\sim 1551\text{ cm}^{-1}$), Amide III ($\sim 1269\text{ cm}^{-1}$; 1273 cm^{-1}), proteins ($\sim 1485\text{ cm}^{-1}$), lipid ($\sim 1717\text{ cm}^{-1}$, 1721 cm^{-1}), COO⁻ symmetric stretching vibrations of fatty acids and amino acid ($\sim 1342\text{ cm}^{-1}$; 1381 cm^{-1}), $\nu_s\text{PO}_2^-$ ($\sim 1069\text{ cm}^{-1}$), $\nu_{\text{as}}\text{PO}_2^-$ ($\sim 1196\text{ cm}^{-1}$) and glycogen ($\sim 1018\text{ cm}^{-1}$) (Figure 6B)⁶⁰. Samples from death-phase cultures exhibit distinct patterns as compared to log- or stationary-phase in that AgNP and tetracycline-AgNP mixture show more impacts on proteins (Figure 6C). These results indicate the changing physiological profiles of bacterial cells with growth stage, and the different modifications associated with cellular components with adaptation to the living environment. For instance, bacteria facing nutrient depletion are reported to produce more hydrophobic molecules to protect the starved cells, resulting in less fluid and permeable membranes attributed to the transformations within the fatty acid composition, which increase protection and insulation from a stressful environment^{20, 61, 62}. Moreover, entering stationary phase, a wide range of protein synthesis is also altered by the global gene regulatory network, which tends to swap the core functions from metabolism or catabolism to the maintenance of cellular viability²⁰, possibly explaining more spectral alterations of proteins in stationary- and death-phase than log-phase.

Besides intrinsic factors, external environmental exposure explains 12.0% of total variation in MRT for Gram-positive (2.7%) and Gram-negative (9.3%) bacteria. For both strains, segregation mainly results from different spectrochemical alterations between AgNP exposure and tetracycline/binary groups. The key spectral alterations in the AgNP category are located at COO⁻ symmetric stretching vibrations of fatty acids and amino acid (~1373 cm⁻¹), (~1736 cm⁻¹), proteins (~984 cm⁻¹, 988 cm⁻¹), Amide I (1612 cm⁻¹, 1694), Amide II (1543 cm⁻¹, 1562 cm⁻¹), and ν_s PO₂⁻ (1088 cm⁻¹) (Figure 3B and 3F)^{36, 60}. In contrast, changes induced by tetracycline or tetracycline-AgNP mixture are associated with COO⁻ symmetric stretching vibrations of fatty acids and amino acid (~1373 cm⁻¹), proteins (~984 cm⁻¹), lipids (~1697 cm⁻¹; 1732 cm⁻¹), and Amide I, II (~1562 cm⁻¹, 1616 cm⁻¹) (Figure 3C and 3G)⁶⁰.

It can be concluded that AgNP-induced spectral changes are mainly associated with proteins, whereas broader cellular components are affected post-exposure to tetracycline or tetracycline-AgNP mixture. It might be explained by tetracycline penetrating cells *via* passive diffusion, which alters bacterial growth by inhibiting protein synthesis or destroying the membrane. Phospho-lipids or proteins are therefore more significantly affected as the primary receptors of passively accumulated tetracycline⁶³. Although mechanisms of AgNP interacting with cytoplasmic membranes and penetrating into cells remain unclear^{58, 65}, our data suggest that AgNP-induced alterations might be derived from some specific active sites interacting with AgNP, *e.g.*, sulfur-containing proteins following a similar mechanism as thiol groups of respiratory chain proteins and transport proteins⁶⁶⁻⁶⁸.

To further assess the impact of exposure, the inter-category multivariate distances of each category were also evaluated. PCA-LDA scores plots that compare the spectrochemical alterations of the two bacterial strains within the same growth phase are shown in Figure 4. The results illustrate distinct clustering of tetracycline exposure away from the control category, but not for AgNP categories, whereas the binary group is located between AgNP and tetracycline categories. The spectral differences of *M. vanbaalenii* between categories of control and binary exposure are slightly reduced within 0.1 as compared to the tetracycline exposure category, indicating that AgNP may confer the exposure effect of tetracycline. Similar alterations are observed for *P. fluorescens*. Additionally, for both *M. vanbaalenii* and *P. fluorescens*, the AgNP and tetracycline categories in the stationary- or death-phase

shift in an opposite direction from the control, and the binary exposure category locates closer to the tetracycline exposure group than control or AgNP exposure. This finding is supported by a range of identical alterations identified in both AgNP and binary exposure groups from stationary-phase to death-phase (*i.e.*, lipids, Amide I, II, III, $\nu_{as}PO_2^-/\nu_sPO_2^-$).

Additionally, the analysis of reactive oxygen species (ROS) was also conducted to evaluate the exposure impacts by calculating the CySS-to-protein ratio, derived from Raman spectra (Figure 7), which points to cellular ROS levels³⁴. Interestingly, comparing to control category, only tetracycline-binary exposure appears to increase ROS level ($P < 0.05$), whereas the induction of AgNP and tetracycline exposure is not significant. Previous studies report the independent mechanisms of antimicrobials on the involvement of ROS^{69, 70}. The results herein hint at no ROS generation from individual AgNP or tetracycline exposure, and the spectrochemical alterations more likely result from the direct inhibition of cell-wall assembly, protein synthesis and DNA replication. In binary exposure, AgNP penetration across the cell membrane might increase permeability and result in more tetracycline entering the bacterial cell, consequently triggering a ROS response^{44, 71-74}.

Conclusions

The present study demonstrates that spectrochemical techniques coupled with multivariate analysis are a robust tool for investigating the bacterial response to environmental exposures, revealing biochemical information longitudinally at low-level exposures. This approach can be applied to characterize and assess bacterial alterations effectively post-exposure to a tetracycline and/or AgNP through growth phases and is potentially feasible for *in situ* interrogation of antimicrobial effects in real-time. Deeper insights into biospectral alterations in non-log phases pertaining nutrient depletion conditions, which fits better with the real-world scenario of microcosms, uncovers the distinct changes of biochemical fingerprints across growth periods, hinting at an underestimation of antimicrobial effects in previous studies. Bacterial type is ranked as the primary factor affecting microbial response to environmental stimuli by MRT analysis, followed by growth phase and types of antimicrobials. These findings will help our better understanding of the real interactions between microbes and low-level antimicrobials under natural environmental conditions, *e.g.*, nutrient depletion.

442

443 **Conflicts of interest**

444 There are no conflicts of interest to declare.

445

446 **Acknowledgement**

447 N.J. was funded by Chinese Academy of Sciences and China Scholarship Council.

448

449 **References**

- 450 1. G. Hamscher, S. Sczesny, H. Höper and H. Nau, *Analytical Chemistry*, 2002,
451 74, 1509-1518.
- 452 2. T. S. TA, *Quintessence Int.*, 1998, **29**, 223-229.
- 453 3. J. C. Chee-Sanford, R. I. Aminov, I. J. Krapac, N. Garrigues-Jeanjean and R. I.
454 Mackie, *Applied and Environmental Microbiology*, 2001, **67**, 1494-1502.
- 455 4. L. Cantas, S. Q. Shah, L. M. Cavaco, C. M. Manaia, F. Walsh, M. Popowska,
456 H. Garelick, H. Burgmann and H. Sorum, *Frontiers in Microbiology*, 2013, **4**,
457 96.
- 458 5. M. Tandukar, S. Oh, U. Tezel, K. T. Konstantinidis and S. G. Pavlostathis,
459 *Environmental Science and Technology*, 2013, **47**, 9730-9738.
- 460 6. J. L. Martinez and F. Baquero, *Upsala Journal Medical Sciences*, 2014, **119**,
461 68-77.
- 462 7. H. H. Lara, N. V. Ayala-Núñez, L. d. C. Ixtepan Turrent and C. Rodríguez
463 Padilla, *World Journal of Microbiology and Biotechnology*, 2009, **26**,
464 615-621.
- 465 8. R. J. Griffitt, N. J. Brown-Peterson, D. A. Savin, C. S. Manning, I. Boube, R.
466 A. Ryan and M. Brouwer, *Environmental Toxicology and Chemistry*, 2012, **31**,
467 160-167.
- 468 9. Y. Kampmann, E. De Clerck, S. Kohn, D. Patchala, R. Langerock and J.
469 Kreyenschmidt, *Journal of Applied Microbiology*, 2008, **104**, 1808-1814.
- 470 10. A. Gupta and S. Silver, *Nature Biotechnology*, 1998, **16**, 888-888.
- 471 11. O. I. Kalantzi, R. Hewitt, K. J. Ford, L. Cooper, R. E. Alcock, G. O. Thomas, J.
472 A. Morris, T. J. McMillan, K. C. Jones and F. L. Martin, *Carcinogenesis*,
473 2004, **25**, 613-622.
- 474 12. J. L. Barber, M. J. Walsh, R. Hewitt, K. C. Jones and F. L. Martin,
475 *Mutagenesis*, 2006, **21**, 351-360.
- 476 13. E. K. Costello, C. L. Lauber, M. Hamady, N. Fierer, J. I. Gordon and R.
477 Knight, *Science*, 2009, **326**, 1694-1697.

- 478 14. C. L. Lauber, M. Hamady, R. Knight and N. Fierer, *Applied and*
479 *Environmental Microbiology*, 2009, **75**, 5111-5120.
- 480 15. P. Marschner, C.-H. Yang, R. Lieberei and D. Crowley, *Soil Biology and*
481 *Biochemistry*, 2001, **33**, 1437-1445.
- 482 16. M. Wietz, B. Wemheuer, H. Simon, H. A. Giebel, M. A. Seibt, R. Daniel, T.
483 Brinkhoff and M. Simon, *Environmental Microbiology*, 2015, **17**, 3822-3831.
- 484 17. J. R. Morones, J. L. Elechiguerra, A. Camacho, K. Holt, J. B. Kouri, J. T.
485 Ramirez and M. J. Yacaman, *Nanotechnology*, 2005, **16**, 2346-2353.
- 486 18. S. M. Ede, L. M. Hafner and P. M. Fredericks, *Applied Spectroscopy*, 2004, **58**,
487 317-322.
- 488 19. J. Monod, *Annual Reviews in Microbiology*, 1949, **3**, 371-394.
- 489 20. R. Kolter, D. A. Siegele and A. Tormo, *Annual Reviews in Microbiology*,
490 1993, **47**, 855-874.
- 491 21. F. Růžicka, V. Holá, M. Votava, R. Tejkalová, R. Horvát, M. Heroldová and
492 V. Woznicová, *Folia Microbiologica*, 2004, **49**, 596-600.
- 493 22. F. Ruzicka, M. Horka, V. Hla and M. Votava, *Journal of Microbiological*
494 *Methods*, 2007, **68**, 530-535.
- 495 23. T. Mathur, S. Singhal, S. Khan, D. Upadhyay, T. Fatma and A. Rattan, *Indian*
496 *Journal of Medical Microbiology*, 2006, **24**, 25.
- 497 24. D. Klug, F. Wallet, S. Kacet and R. J. Courcol, *Journal of Clinical*
498 *Microbiology*, 2003, **41**, 3348-3350.
- 499 25. P. Vasudevan, M. K. M. Nair, T. Annamalai and K. S. Venkitanarayanan,
500 *Veterinary Microbiology*, 2003, **92**, 179-185.
- 501 26. E. Muñoz-Atienza, C. Araújo, R. del Campo, P. E. Hernández, C. Herranz and
502 L. M. Cintas, *LWT-Food Science and Technology*, 2016, **65**, 357-362.
- 503 27. F. C. Tenover, R. D. Arbeit, R. V. Goering, P. A. Mickelsen, B. E. Murray, D.
504 H. Persing and B. Swaminathan, *Journal of Clinical Microbiology*, 1995, **33**,
505 2233.
- 506 28. E. E. Vaughan, F. Schut, H. Heilig, E. G. Zoetendal, W. M. de Vos and A. D.
507 Akkermans, *Current Issues in Intestinal Microbiology*, 2000, **1**, 1-12.

- 508 29. M. Espy, J. Uhl, L. Sloan, S. Buckwalter, M. Jones, E. Vetter, J. Yao, N.
509 Wengenack, J. Rosenblatt and F. Cockerill, *Clinical Microbiology Reviews*,
510 2006, **19**, 165-256.
- 511 30. D. Klein, *Trends in Molecular Medicine*, 2002, **8**, 257-260.
- 512 31. J. Heber, R. Severson and O. Boldman, *Science*, 1952, **116**, 11.
- 513 32. K. Norris, *Journal of Hygiene*, 1959, **57**, 326-345.
- 514 33. M. J. Baker, J. Trevisan, P. Bassan, R. Bhargava, H. J. Butler, K. M. Dorling,
515 P. R. Fielden, S. W. Fogarty, N. J. Fullwood, K. A. Heys, C. Hughes, P. Lasch,
516 P. L. Martin-Hirsch, B. Obinaju, G. D. Sockalingum, J. Sule-Suso, R. J.
517 Strong, M. J. Walsh, B. R. Wood, P. Gardner and F. L. Martin, *Nature*
518 *Protocols*, 2014, **9**, 1771-1791.
- 519 34. J. Li, R. Strong, J. Trevisan, S. W. Fogarty, N. J. Fullwood, K. C. Jones and F.
520 L. Martin, *Environmental Science and Technology*, 2013, **47**, 10005-10011.
- 521 35. F. L. Martin, J. G. Kelly, V. Llabjani, P. L. Martin-Hirsch, I. I. Patel, J.
522 Trevisan, N. J. Fullwood and M. J. Walsh, *Nature Protocols*, 2010, **5**,
523 1748-1760.
- 524 36. K. A. Heys, M. J. Riding, R. J. Strong, R. F. Shore, M. G. Pereira, K. C. Jones,
525 K. T. Semple and F. L. Martin, *Analyst*, 2014, **139**, 896-905.
- 526 37. J. Schmitt and H.-C. Flemming, *Int Biodeterior Biodegradation*, 1998, **41**,
527 1-11.
- 528 38. A. Bosch, D. Serra, C. Prieto, J. Schmitt, D. Naumann and O. Yantorno,
529 *Applied Microbiology and Biotechnology*, 2006, **71**, 736-747.
- 530 39. J. J. Ojeda, M. E. Romero-González, R. T. Bachmann, R. G. Edyvean and S.
531 A. Banwart, *Langmuir*, 2008, **24**, 4032-4040.
- 532 40. S. J. Clarke, R. E. Littleford, W. E. Smith and R. Goodacre, *Analyst*, 2005,
533 **130**, 1019-1026.
- 534 41. N. Pradhan, S. K. Pradhan, B. B. Nayak, P. S. Mukherjee, L. B. Sukla and B.
535 K. Mishra, *Research in Microbiology*, 2008, **159**, 557-561.
- 536 42. I. Chopra and M. Roberts, *Microbiology and Molecular Biology Reviews*,
537 2001, **65**, 232-260.

- 538 43. M. D. Barton, *Nutrition Research Reviews*, 2000, **13**, 279-299.
- 539 44. A. M. Fayaz, K. Balaji, M. Girilal, R. Yadav, P. T. Kalaichelvan and R.
540 Venketesan, *Nanomedicine*, 2010, **6**, 103-109.
- 541 45. P. Li, J. Li, C. Wu, Q. Wu and J. Li, *Nanotechnology*, 2005, **16**, 1912.
- 542 46. S.-J. Kim, O. Kweon, R. C. Jones, J. P. Freeman, R. D. Edmondson and C. E.
543 Cerniglia, *Journal of Bacteriology*, 2007, **189**, 464-472.
- 544 47. J.-S. Seo, Y.-S. Keum and Q. X. Li, *International Journal of Environmental*
545 *Research and Public Health*, 2009, **6**, 278-309.
- 546 48. L. S. Thomashow and D. M. Weller, *Journal of Bacteriology*, 1988, **170**,
547 3499-3508.
- 548 49. R. Hirsch, T. Ternes, K. Haberer and K.-L. Kratz, *Science of the Total*
549 *Environment*, 1999, **225**, 109-118.
- 550 50. R. Hirsch, T. A. Ternes, K. Haberer, A. Mehlich, F. Ballwanz and K.-L. Kratz,
551 *Journal of Chromatography A*, 1998, **815**, 213-223.
- 552 51. G. Artiaga, K. Ramos, L. Ramos, C. Cámara and M. Gómez-Gómez, *Food*
553 *Chemistry*, 2015, **166**, 76-85.
- 554 52. T. Silva, L. R. Pokhrel, B. Dubey, T. M. Tolaymat, K. J. Maier and X. Liu,
555 *Science of the Total Environment*, 2014, **468**, 968-976.
- 556 53. J. Trevisan, P. P. Angelov, A. D. Scott, P. L. Carmichael and F. L. Martin,
557 *Bioinformatics*, 2013, **29**, 1095-1097.
- 558 54. F. L. Martin, M. J. German, E. Wit, T. Fearn, N. Ragavan and H. M. Pollock,
559 *Journal of Computational Biology*, 2007, **14**, 1176-1184.
- 560 55. M. Paraskevaidi, C. L. M. Morais, K. M. G. Lima, J. S. Snowden, J. A. Saxon,
561 A. M. T. Richardson, M. Jones, D. M. A. Mann, D. Allsop, P. L.
562 Martin-Hirsch and F. L. Martin, *Proceedings of the National Academy of*
563 *Sciences USA*, 2017, **114**, E7929-E7938.
- 564 56. M. J. Riding, F. L. Martin, J. Trevisan, V. Llabjani, I. I. Patel, K. C. Jones and
565 K. T. Semple, *Environmental Pollution*, 2012, **163**, 226-234.
- 566 57. J. Li, G. G. Ying, K. C. Jones and F. L. Martin, *Analyst*, 2015, **140**,
567 2687-2695.

- 568 58. I. Sondi and B. Salopek-Sondi, *J. Colloid Interface Sci.*, 2004, **275**, 177-182.
- 569 59. F. Pomati, A. G. Netting, D. Calamari and B. A. Neilan, *Aquatic Toxicology*,
570 2004, **67**, 387-396.
- 571 60. Z. Movasaghi, S. Rehman and D. I. ur Rehman, *Applied Spectroscopy Reviews*,
572 2008, **43**, 134-179.
- 573 61. J. C. Betts, P. T. Lukey, L. C. Robb, R. A. McAdam and K. Duncan,
574 *Molecular Microbiology*, 2002, **43**, 717-731.
- 575 62. T. Hampshire, S. Soneji, J. Bacon, B. W. James, J. Hinds, K. Laing, R. A.
576 Stabler, P. D. Marsh and P. D. Butcher, *Tuberculosis*, 2004, **84**, 228-238.
- 577 63. D. Schnappinger and W. Hillen, *Archives of Microbiology*, 1996, **165**,
578 359-369.
- 579 64. G. D. Shockman, J. J. Kolb and G. Toennies, *Journal of Biological Chemistry*,
580 1958, **230**, 961-977.
- 581 65. C. Marambio-Jones and E. M. Hoek, *Journal of Nanoparticle Research*, 2010,
582 **12**, 1531-1551.
- 583 66. O. Gordon, T. V. Slenters, P. S. Brunetto, A. E. Villaruz, D. E. Sturdevant, M.
584 Otto, R. Landmann and K. M. Fromm, *Antimicrobial Agents and*
585 *Chemotherapy*, 2010, **54**, 4208-4218.
- 586 67. A. J. Kowaltowski and A. E. Vercesi, *Free Radical Biology and Medicine*,
587 1999, **26**, 463-471.
- 588 68. J. F. Turrens, *Bioscience Reports*, 1997, **17**, 3-8.
- 589 69. Y. Liu and J. A. Imlay, *Science*, 2013, **339**, 1210-1213.
- 590 70. I. Keren, Y. Wu, J. Inocencio, L. R. Mulcahy and K. Lewis, *Science*, 2013,
591 **339**, 1213-1216.
- 592 71. H. H. Lara, N. V. Ayala-Núñez, L. d. C. Ixtapan Turrent and C. Rodríguez
593 Padilla, *World Journal of Microbiology and Biotechnology*, 2010, **26**,
594 615-621.
- 595 72. Z.-M. Xiu, J. Ma and P. J. Alvarez, *Environ Sci Technol*, 2011, **45**, 9003-9008.
- 596 73. J. R. Morones, J. L. Elechiguerra, A. Camacho, K. Holt, J. B. Kouri, J. T.
597 Ramírez and M. J. Yacaman, *Nanotechnology*, 2005, **16**, 2346.

598 74. D. Trachootham, Y. Zhou, H. Zhang, Y. Demizu, Z. Chen, H. Pelicano, P. J.
599 Chiao, G. Achanta, R. B. Arlinghaus and J. Liu, *Cancer Cell*, 2006, **10**,
600 241-252.

601

602

Figure Cations

Figure 1. Growth curves of *M. vanbaalenii* (A) and *P. fluorescens* (B) under AgNP, tetracycline and AgNP-tetracycline binary exposures. The exposure concentrations were 4 µg/L for AgNP and 1 µg/L for tetracycline. IR spectral average of *M. vanbaalenii* (C) and *P. fluorescens* (D) in different exposure treatments. The groups of “Log control”, “Log silver”, “Log tet” and “Log binary” refer to samples collected at log-phase following treatments of control, silver, tetracycline and binary-exposure, respectively.

Figure 2. Exposure effects within different growth phases (scale range of Y axis: -0.2 ~ 0.2). The Y axis refers to the values of LD1. *M. vanbaalenii*: control (A), post-exposure to AgNP (B), post-exposure to tetracycline (C), and post-exposure to AgNP-tetracycline mixture (D). *P. fluorescens*: control (E), post-exposure to AgNP (F), post-exposure to tetracycline (G), and post-exposure to AgNP-tetracycline mixture (H).

Figure 3. Vector-cluster analysis of exposure effects within different growth phases. *M. vanbaalenii*: control (A), post-exposure to AgNP (B), post-exposure to tetracycline (C), and post-exposure to AgNP-tetracycline mixture (D). *P. fluorescens*: control (E), post-exposure to AgNP (F), post-exposure to tetracycline (G), and post-exposure to AgNP-tetracycline mixture (H).

Figure 4. Exposure effects within the same growth phase. The Y axis refers to the values of LD1 in range of -0.2 to 0.2. *M. vanbaalenii*: log-phase (A), stationary-phase (B), and death-phase (C). *P. fluorescens*: log-phase (D), stationary-phase (E), and death-phase (F).

Figure 5. Multivariate regression tree (MRT) analysis of environmental variables explaining the discriminating biomarkers. The scale of the sub-figures represents the alteration degree (1.0 refers to the average level). Blue bars for wavelengths representing proteins, yellow bars for phospholipid-derived fatty acids, and grey bars for other cellular components.

Figure 6. Vector-cluster analysis of exposure effects within the same growth phase. *M. vanbaalenii*: log-phase (A), stationary-phase (B), and death-phase (C). *P. fluorescens*: log-phase (D), stationary-phase (E), and death-phase (F).

634 **Figure 7.** Ratio of cysteine (CySS, 668 cm^{-1}) to protein (1447 cm^{-1}) derived from
635 Raman spectra. Data are presented in mean \pm standard error.

636

Figure 1

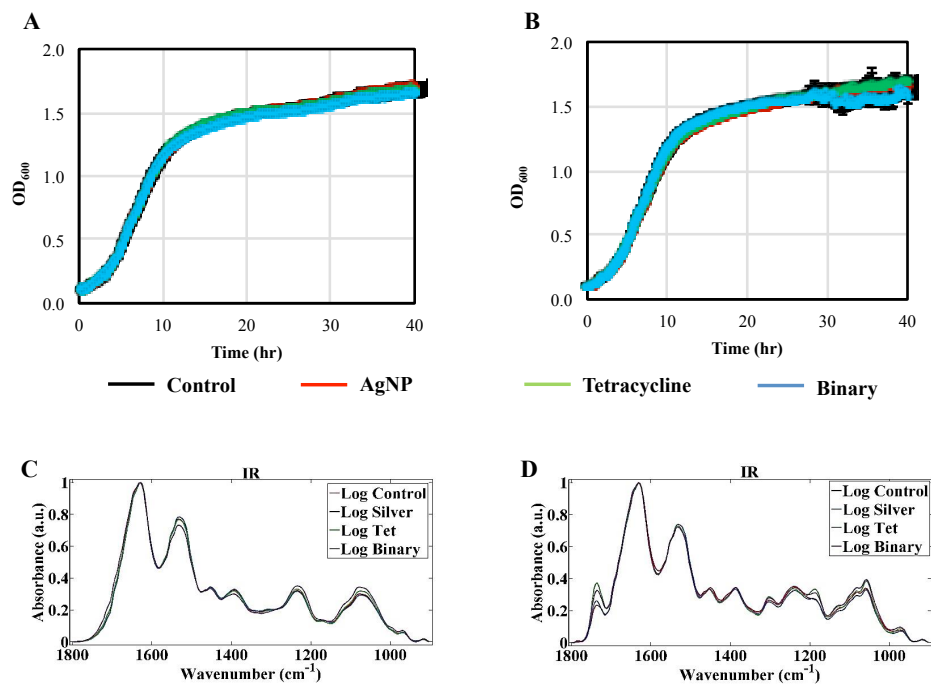


Figure 2

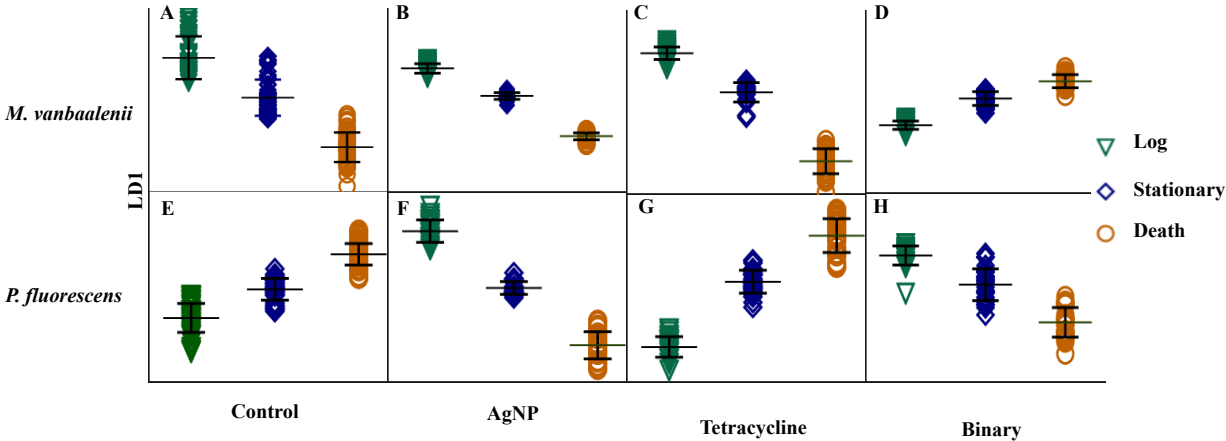


Figure 3

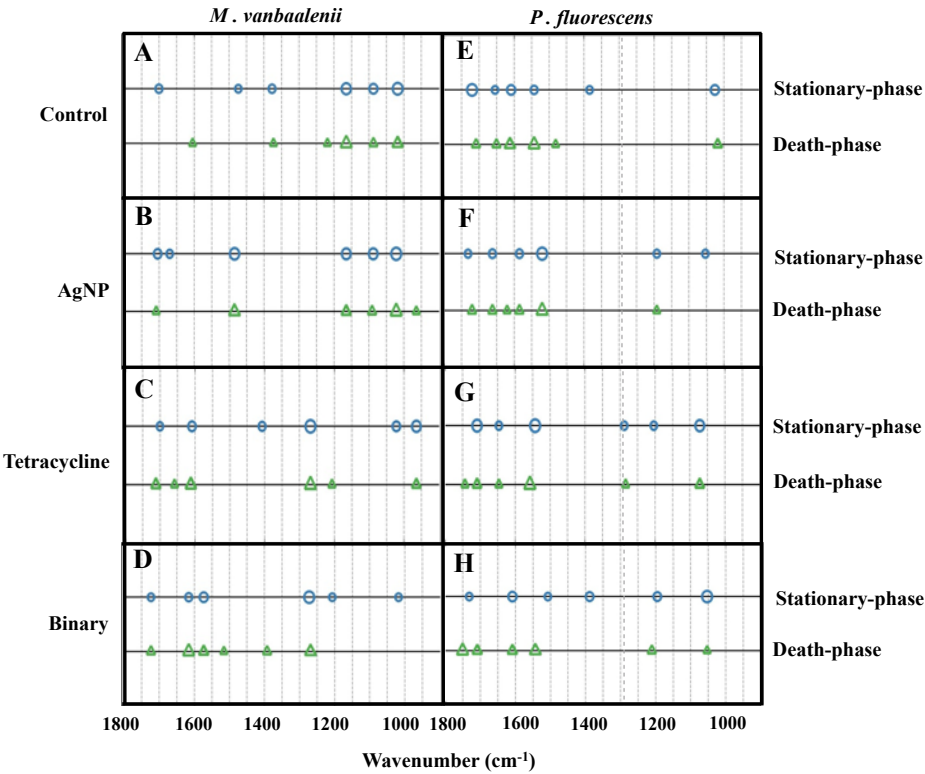


Figure 4

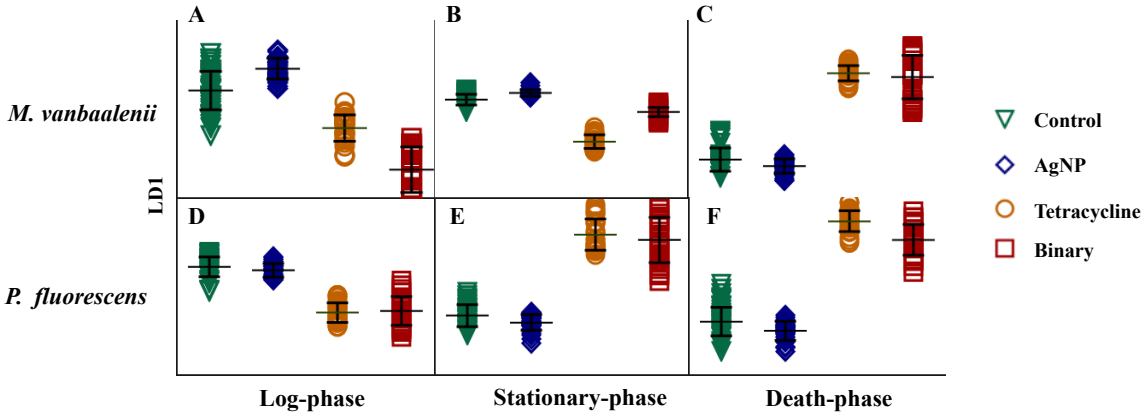


Figure 5

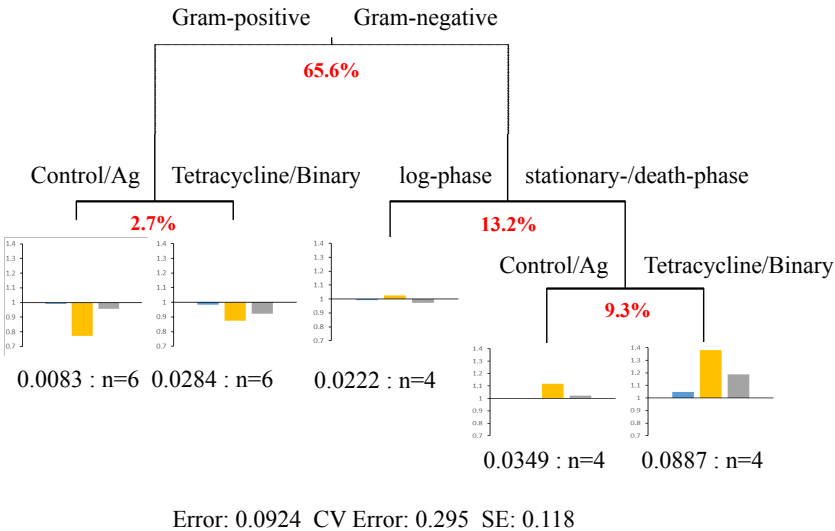


Figure 6

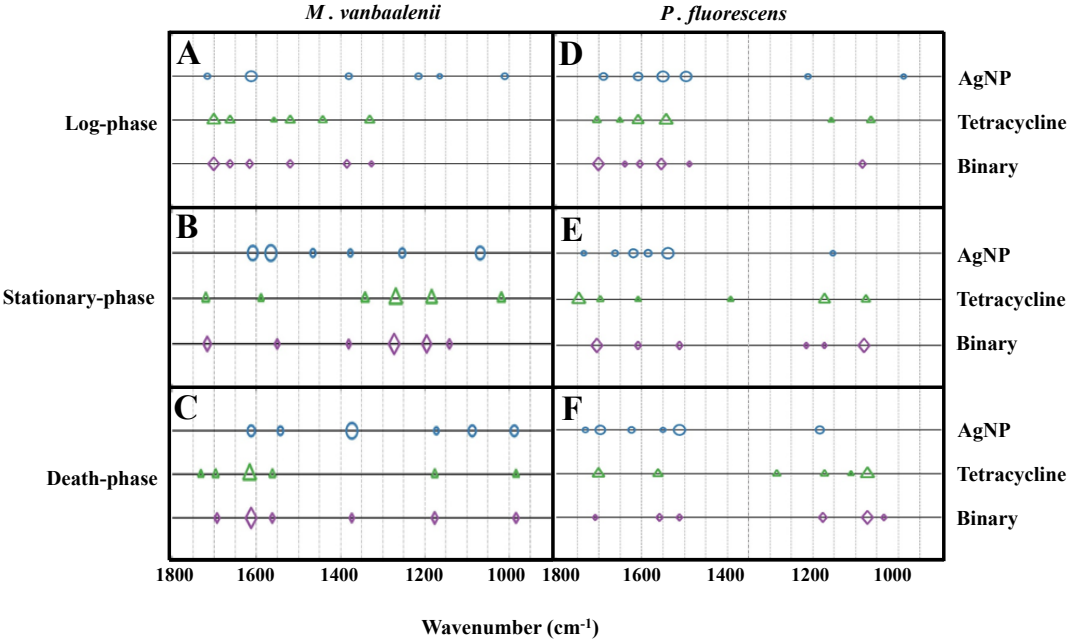


Figure 7

